Journal of Zhejiang University-SCIENCE A (Applied Physics & Engineering)
ISSN 1673-565X (Print); ISSN 1862-1775 (Online)
www.zju.edu.cn/jzus; www.springerlink.com
E-mail: jzus@zju.edu.cn

Simulation of stochastic wind field for large complex structures based on modified Fourier spectrum*

Zhao-dong XU†[1,2], Deng-xiang WANG[1,2], Ke-yi WU[1,2]

([1]*Key Laboratory of C & PC Structures of the Ministry of Education, Southeast University, Nanjing 210096, China*)

([2]*Civil Engineering College, Southeast University, Nanjing 210096, China*)

†E-mail: xuzhdgyq@seu.edu.cn

Received May 3, 2010; Revision accepted Sept. 10, 2010; Crosschecked Jan. 25, 2011

Abstract: Simulation for stochastic wind field is very important in analyzing dynamic responses of large complex structures due to strong wind. The typical simulation method is the spectrum representation method (SRM), but the SRM has drawbacks of inferior precision in lower frequency and slow calculating speed. In view of this, the modified Fourier spectrum method (MFSM) is introduced into the simulation of stochastic wind field in this paper. In this method, phase information of wind velocity time history is determined by cross power spectral density (CPSD) between adjacent points, and the wind velocity time history with time and space correlation is generated by iterative modification for CPSD considering auto power spectral density (APSD). Simulation of the wind field for a long-span bridge is undertaken to verify the effectiveness of the MFSM. Simulation results of the SRM and the MFSM are compared. It can be concluded that the MFSM is more accurate and has higher calculation speed than the SRM.

Key words: Modified Fourier spectrum, Stochastic wind field, Large complex structures, Numerical simulation
doi:10.1631/jzus.A1000209 **Document code:** A **CLC number:** TU393.3

1 Introduction

Wind hazard is one kind of natural disaster with a huge destructive power. In recent years, wind hazard has become a more serious problem due to global warming, and leads to a loss of tens or hundreds of billion dollars per year to the global economy. With the development of construction techniques, civil engineering structures become larger, higher, and lighter, i.e., high-rise buildings, high-tower buildings, long-span space structures, and bridges. All such structures are really sensitive to wind excitation, and static analysis under wind loads is not suitable for structural design and corresponding safety targets. Therefore, dynamic analysis of these structures under wind loads is becoming more and more significant. A time-domain analysis method is usually applied in dynamic analysis under wind loads; i.e., a dynamic differential equation is often solved in time-domain directly, which provides evidence for structural design and fatigue analysis, but wind velocity time history around structures should be determined before time-domain dynamic analysis. Subsequently, the wind velocity time history should be changed into wind pressure time history based on the wind pressure distribution characteristics on the structural surface (Lazzari *et al*., 2003; Mazanoglu *et al*., 2009; Moustafa and Takewak, 2009; Li *et al.*, 2011).

Currently, the main means of wind field acquirement are field measurement, wind tunnel tests and numerical simulation. Field measurement is an important method with high accuracy for studying the wind field characteristics of structures. Many test

* Project supported by the National Natural Science Foundation of China (No. 90915004), the Six Talents Peak in Jiangsu Province (No.2008178), and the 333 High-Level Talent Training Project of Jiangsu Province, China

works for the wind field were undertaken. Davenport (1961) proposed the Davenport spectrum based on more than 90 strong wind records in different cites and at different heights around the world. He also proposed that the turbulence integral length scale of the horizontal wind velocity spectrum is invariable along the height. Kaimal *et al*. (1972) proposed the Kaimal spectrum based on some strong wind field test records，and also proposed that the turbulence integral length scale is invariable along the height. Xu *et al*. (2001) and Miyata *et al*. (2001) undertook long time tests of Tsing Ma Bridge in Hong Kong (China) and Akashi Bridge in Japan, respectively. However, field measurements are uneconomic and laborious. Therefore, field measurements are limited in wind field acquirement. A wind tunnel test is another important method for wind field acquirement. Wind field characteristics, which can provide important evidence for vibration analysis, can be obtained by a wind tunnel test. However, a wind tunnel test is also expensive and labor-intensive. Moreover, a wind tunnel test is limited due to diverse wind field, complex structure shape, and inaccurate Reynolds parameter for scaled model structures. Generally, wind velocity time history is generated according to wind velocity spectrums with special characteristics, such as the Davenport spectrum, the Kaimal spectrum, and the Harris spectrum, which are summarized based on strong wind records. Such wind velocity spectrums are very representative and accurate, and can satisfy the demands of simulation for wind velocity time history and dynamic analysis. Currently, spectrum representation method (SRM) and autoregressive method (ARM) are usually applied in simulation of stochastic wind field. Shinozuka and Jan (1972) proposed the SRM, which is accurate but time-consuming; i.e., a history of cosine functions is adopted to simulate random process. Deodatis (1996) proposed the conception of double index of frequency, which improves the simulation accuracy. The ARM is based on a linear filtering technique; i.e., white noise is passed through a filter, and a random process with a special spectrum is exported as the simulation of the wind field.

The ARM is efficient with little calculation, and has fast calculation speed, but less accuracy compared to the SRM. In fact, the precision of the SRM usually does not meet the calculating requirement. Moreover, SRM has the drawback of a slow calculation speed. A new method named the modified Fourier spectrum method (MFSM) is introduced into the simulation of stochastic wind field in this paper. Phase information of a simulated point is determined by cross power spectral density (CPSD) between the simulation and the adjacent points. Combined with the auto power spectral density (APSD) of the simulation point, iterative modification for Fourier spectrum is carried out, and wind velocity time history with special time and space correlation is generated. Simulation of the wind field for a long-span bridge is undertaken by numerical analysis. In the analysis, the Kaimal spectrum is adopted as the target spectrum and Davenport form is adopted as the correlation function. A comparison study for simulated results between the SRM and the MFSM is also undertaken. It can be concluded that the MFSM has an excellent accuracy and a high calculation speed (about 5 times faster than the SRM). This will be beneficial for the simulation of the wind field and wind vibration analysis for large complex structures.

2 Spectral representation method

The SRM was initially used to simulate a stationary Gauss random process with a single variable. Subsequently, SRM was developed to simulate a non-stationary Gauss random process with multi-variables.

Space characteristics of the wind field should be determined firstly in order to simulate the wind velocity time history, which is often seen as a 3D random process with multi-variables. The 3D wind field in Cartesian coordinates can be expressed as

$$\begin{cases} U = \overline{U}(z) + u(y,z,t), \\ v = v(y,z,t), \\ w = w(y,z,t), \end{cases} \tag{1}$$

where U is the velocity of the wind flow in the longitudinal direction, $\overline{U}$ is the average wind velocity in the longitudinal direction, μ, v, and w are wind velocity components in the longitudinal, lateral, and gravity directions, respectively, and t is the time variable. Average wind velocity $\overline{U}(z)$ is an important

index describing the distribution of wind field about height, which conforms to the law of logarithm:

$$\overline{U}(z)=\frac{1}{k}v_{\mathrm{f}}\ln(z/z_0), \tag{2}$$

where the Kaman constant k=0.4, z_0 is the roughness length, and v_{f} is the friction velocity.

The power spectral density is usually used to describe energy characteristics of the wind field, such as the Davenport spectrum, the Kaimal spectrum, and the Harris spectrum. The Kaimal spectrum can be expressed as

$$\frac{\omega S(f)}{v_{\mathrm{f}}^2}=\frac{200f}{(1+50f)^{5/3}}, \tag{3}$$

where $S(f)$ and ω are the power spectral density and frequency, respectively. $f=\dfrac{\omega z}{\overline{U}(z)}$ is a non-dimensional Monin coordinate.

Space correlation exists in wind excitation to structures, which is a function of the distance between space points, and can be expressed by the correlation coefficient (i.e., Coh(ω)) in accordance with the Davenport form

$$\mathrm{Coh}(\omega)=\exp\left(-C\frac{\omega r}{2\pi\overline{U}(z)}\right), \tag{4}$$

where C, ω, and r are the attenuation coefficient, frequency, and distance of space points, respectively. At the same time, the CPSD of each point can be expressed as

$$\begin{aligned}&S_{ij}(\omega)=\sqrt{S_{ii}(\omega)S_{jj}(\omega)}\mathrm{Coh}_{ij}(\omega)\exp[\mathrm{i}\phi(\omega)],\\&\quad i,\,j=1,\,2,\ldots,m,\end{aligned} \tag{5}$$

where $\phi(\omega)$ is the phase deviation.

For the SRM, the stationary Gauss random process can be simulated by a combination of different trigonometric functions. Supposing m points wind velocity time histories are required to be simulated, m stationary Gauss random processes (i.e., $u_i^0(t)$) with an average value of zero will be obtained, and the matrix of CPSD can be expressed as

$$\boldsymbol{S}^0(\omega)=\begin{bmatrix}S_{11}^0(\omega) & S_{12}^0(\omega) & \cdots & S_{1m}^0(\omega)\\ S_{21}^0(\omega) & S_{22}^0(\omega) & \cdots & \cdots\\ \vdots & \vdots & \vdots & \vdots\\ S_{m1}^0(\omega) & S_{m2}^0(\omega) & \cdots & S_{mm}^0(\omega)\end{bmatrix}, \tag{6}$$

where $S_{ii}^0(\omega)$ is APSD with the form of real number, and $S_{ij}^0(\omega)\ (i\neq j)$ $(i,j=1,2,\ldots,m)$ is the CPSD with the form of complex number. The Cholesky decomposition is undertaken on $\boldsymbol{S}^0(\omega)$:

$$\boldsymbol{S}^0(\omega)=\boldsymbol{H}(\omega)\boldsymbol{H}^{*\mathrm{T}}(\omega), \tag{7}$$

where $\boldsymbol{H}(\omega)$ is a lower triangular matrix, $\boldsymbol{H}^{*\mathrm{T}}(\omega)$ is the complex conjugated transpose matrix of $\boldsymbol{H}(\omega)$. $\boldsymbol{H}(\omega)$ can be expressed as

$$\boldsymbol{H}(\omega)=\begin{bmatrix}H_{11}(\omega) & 0 & \cdots & 0\\ H_{21}(\omega) & H_{22}(\omega) & \cdots & 0\\ \vdots & \vdots & \vdots & \vdots\\ H_{m1}(\omega) & H_{m2}(\omega) & \cdots & H_{mm}(\omega)\end{bmatrix}. \tag{8}$$

In accordance with the property of an auto correlation function, diagonal elements will satisfy the following equation:

$$H_{ii}(\omega)=H_{ii}(-\omega). \tag{9}$$

For non-diagonal elements, the following equation will be satisfied:

$$H_{ij}(\omega)=\left|H_{ij}^*(-\omega)\right|\mathrm{e}^{\mathrm{i}\theta_{ij}(\omega)}, \tag{10}$$

where $\theta_{ij}(\omega)=\arctan\dfrac{\mathrm{Im}\left[H_{ij}(\omega)\right]}{\mathrm{Re}\left[H_{ij}(\omega)\right]}$, which is the phase of different points.

According to the theory of Shinozuka and Jan (1972), the wind velocity time history can be simulated as

$$u_i(t)=\sum_{j=1}^{i}\sum_{k=1}^{N}\left|H_{ij}(\omega_k)\right|\sqrt{2\Delta\omega}\cos[\omega_k t-\theta_{ij}(\omega_k)+\varphi_{jk}], \tag{11}$$

where N, $\Delta\omega$, and φ_{jk} are points quantity within limit frequency, frequency interval, and phase with uniform distribution with the range of 0–2π, respectively, and ω_k, which is the frequency of the kth point, can be expressed based on the concept of double index of frequency (Samaras *et al*., 1985) as

$$\omega_k = (j-1)\Delta\omega + \frac{m}{N}\Delta\omega. \tag{12}$$

Additionally, points quantity within limit time must be above $2N$, and the time interval must be below π/ω_u. ω_u is the upper bound of the simulate frequency, and it can be estimated as

$$\int_0^{\omega_u} S(\omega)\mathrm{d}\omega = (1-\xi)\int_0^{\infty} S(\omega)\mathrm{d}\omega, \tag{13}$$

where ξ is a real number.

The stability and accuracy of the solution obtained by Eq. (11) can satisfy the simulation request only if Eqs. (12) and (13) are satisfied (Samaras *et al*., 1985). Chondros and Dimarogonas (1989) introduced changes of dynamic characteristics including natural frequency and mode shapes with the changes of stiffness due to cracks of concrete, which is derived by eigenvalues and eigenvectors.

In accordance with Eq. (11), wind velocity time histories of all points can be simulated, whenever the target spectrum matrix $\boldsymbol{S}^0(\omega)$ is determined.

3 Modified Fourier spectrum method

As described above, the SRM is not usually satisfactory for wind field simulation due to its low efficiency and insufficient precision for some simulations (Backström and Nilsson, 2007; Mason *et al*., 2009). To solve these problems, a new simulation method based on the modified Fourier spectrum is introduced to simulate stochastic wind field in this study. The MFSM is a classical method simulating earthquake waves (Wang and Hu, 2006). In this method, earthquake waves are generated in accordance with a target response spectrum. It is known that stochastic wind has the determined power spectrum (i.e., target response spectrum) (Islam *et al*., 2009). Based on the same idea of the generation of earthquake waves, the wind velocity time history can be generated by the MFSM. In the simulation of earth-quake waves, the MFSM does not take time and space correlation into consideration. For the simulation of the wind field in this study, the calculating process of the initial MFSM for simulation of earthquake waves is adjusted; i.e., the power spectral density of the wind velocity time history considers time and space correlation.

3.1 Determination of the phase information with correlation

For the SRM, as shown in Eq. (6), the Cholesky decomposition is required to be undertaken for the power spectral density matrix $\boldsymbol{S}^0(\omega)$ in order to obtain $\boldsymbol{H}(\omega)$, which will be used to determine phase information. Cholesky decomposition has low calculation efficiency, and decomposition cannot always be performed because of the singularity of $\boldsymbol{S}^0(\omega)$. In the MFSM, phase information of a simulated point is determined by CPSD between this point and the adjacent point. Combined with the APSD, wind velocity time history can be simulated, and the Cholesky decomposition is avoided, which has great efficiency and excellent accuracy.

$\boldsymbol{S}^0(\omega)$ is the same for all simulation points, i.e., $S_{ii}^0(\omega) = S_{11}^0(\omega)$ (i=1, 2, …, m). Wind velocity time history of the first point can be generated in accordance with its APSD $S_{11}^0(\omega)$, for example, the APSD of the second point $S_{22}^0(\omega)$ is equal to $S_{11}^0(\omega)$, and the phase information $\phi_2(\omega)$ can be determined by the CPSDs $S_{21}^0(\omega)$ and $S_{22}^0(\omega)$. By the same means, APSD of the ith point $S_{ii}^0(\omega)$ is also equal to $S_{11}^0(\omega)$, and the phase information $\phi_i(\omega)$ can be determined by $S_{i,i-1}^0(\omega)$ and $S_{ii}^0(\omega)$. Supposing $L_{ii}(\omega) = \sqrt{S_{ii}^0(\omega)} = \sqrt{S_{11}^0(\omega)}$, the modified function of phase can be expressed as

$$L_i(\omega) = S_{i,i-1}^0(\omega)\big/L_{ii}(\omega) = S_{i,i-1}^0(\omega)\big/\sqrt{S_{11}^0(\omega)}, \tag{14}$$

and the phase can be expressed as

$$\phi_i(\omega) = \arctan\frac{\mathrm{Im}\left[L_i(\omega)\right]}{\mathrm{Re}\left[L_i(\omega)\right]}. \tag{15}$$

Consequently, the phase information matrix $\boldsymbol{\phi}(\omega)$ can be constructed as

$$\boldsymbol{\phi}(\omega)=[\phi_1(\omega)\ \cdots\ \phi_i(\omega)\ \cdots\ \phi_m(\omega)]. \tag{16}$$

3.2 Simulation of stochastic wind field

The target power spectral density matrix can be obtained based on Eqs. (1)–(5). Fourier spectrum $A_{ii}(\omega)$ can be estimated as follows according to APSD (i.e., $S_{ii}(\omega)$):

$$A_{ii}(\omega)=\left[\frac{4S_{ii}(\omega)\cdot 2\pi\cdot f_s}{\text{nfft}}\right]^{1/2}, \tag{17}$$

where f_s is the sampling frequency of simulating wind velocity time history, and nfft is the number of points of Fourier transformation. $\phi_i(\omega)$ can be obtained by Eq. (15), and then the Fourier spectrum can be changed into a complex form combined with $\phi_i(\omega)$:

$$C_{ii}^k(\omega)=A_{ii}^k(\omega)\mathrm{e}^{\mathrm{i}\phi(\omega)}. \tag{18}$$

The inverse fast Fourier transform (IFFT) is undertaken for $\boldsymbol{C}(\omega)$, which is the combination of $C_{ii}(\omega)$, and then the wind velocity time history $Y_i^k(t)$ is generated based on the real part of the inverse fast Fourier transform result:

$$y_i^k(t)=\text{IFFT}(C_{ii}^k(\omega)), \tag{19}$$

$$Y_i^k(t)=\text{RE}(y_i^k(t)). \tag{20}$$

The APSD of $Y_i(t)$ can be calculated by

$$S_{ii}^{k'}(\omega)=\text{PSD}(Y_i^k(t)). \tag{21}$$

The new Fourier spectrum $A_{ii}^{k'}(\omega)$ of $Y_i^k(t)$ can be calculated by

$$A_{ii}^{k'}(\omega)=\left[\frac{4S_{ii}^{k'}(\omega)\cdot 2\pi\cdot f_s}{\text{nfft}}\right]^{1/2}. \tag{22}$$

Then, the previous Fourier spectrum $A_{ii}^k(\omega)$ should be modified by the ratio between $A_{ii}(\omega)$ and $A_{ii}^{k'}(\omega)$:

$$A_{ii}^{k+1}(\omega)=A_{ii}^k(\omega)\times\frac{A_{ii}(\omega)}{A_{ii}^{k'}(\omega)}. \tag{23}$$

Finally, $A_{ii}^k(\omega)$ in Eq. (22) is substituted by $A_{ii}^{k+1}(\omega)$, and the wind velocity time history is obtained in accordance with the given iteration times.

The total calculating process of the MFSM could be summarized as follows (Fig. 1). Firstly, the target power spectral density $S_{ii}(\omega)$ can be calculated by Eqs. (1)–(5) based on the previous $\phi_i(\omega)$, and then the phase deviation $\phi_i(\omega)$ is obtained by Eqs. (14) and (15) based on $S_{ii}(\omega)$. Secondly, Fourier spectrum $A_{ii}(\omega)$ can be estimated by Eq. (17) and then is transformed to a complex form $\boldsymbol{C}(\omega)$ by Eq. (18). Finally, an inverse fast Fourier transform is calculated

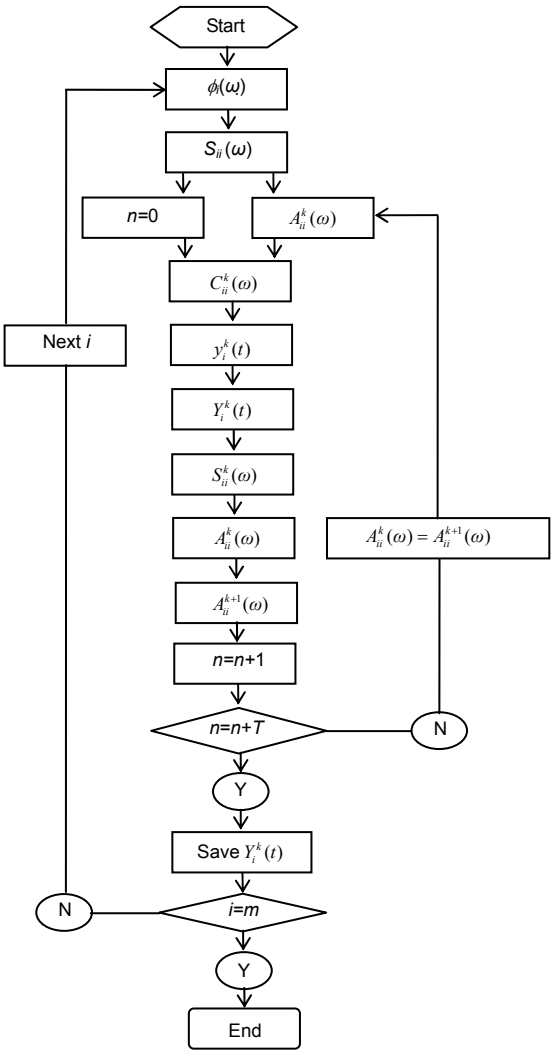

Fig. 1 Process of the modified Fourier spectrum method

for $\boldsymbol{C}(\omega)$, and the wind velocity time history $Y_i^k(t)$ is generated based on the real part of the inverse fast Fourier transform result. Then $A_{ii}^k(\omega)$ in Eq. (22) is substituted by $A_{ii}^{k+1}(\omega)$ in Eq. (23). Go to step 2 and start a new calculation. Iterative calculation is continued until the given time period T is completed, and thus the wind velocity time history will be obtained.

4 Numerical analysis

To verify the effectiveness of the MFSM, simulation of the wind field for a long-span bridge is undertaken, and simulation results between the MFSM and SRM are compared. The span of the bridge is 1000 m, and the height of the deck is 50 m. Average wind velocity at the point of 10 m in the height is 40 m/s, and the landform category is A (GB 50009-2001). The number of simulating points is 10 with the number ranging from 1–10 distributed evenly along the deck at intervals of 100 m. In the numerical example, the target spectrum uses the Kaimal spectrum, and the correlation function uses the Davenport form with the attenuation coefficient C=10. The upper limit frequency of the simulating wind velocity time history is 2 Hz, the sampling frequency is 4 Hz, and the total sampling time is 1000 s.

Wind velocity time history curves of the 10 simulating points are simulated by the MFSM and SRM. Figs. 2 and 3 show the wind velocity time history curves of the 1st and the 10th points obtained by the MFSM and the SRM, respectively.

To show the frequency spectrum characteristics of the wind velocity time histories of the 1st and the 10th points, the APSD of the 1st and the 10th points can be obtained using the MFSM and the SRM (Figs. 4 and 5). Fig. 4 shows that the APSD of the wind velocity time history simulated by the MFSM fits well with the target power spectrum densities, while the APSD of the wind velocity time history simulated by the SRM does not fit well with the target power spectrum densities (Fig. 5). There is an obvious difference in the lower frequency area between the two spectrum curves, and the APSD of wind velocity time history simulated by SRM shows strong oscillation characteristics in the higher frequency area (Fig. 5). Obviously, the precision of the MFSM is much higher than the SRM in simulation for the APSD of the wind velocity time history.

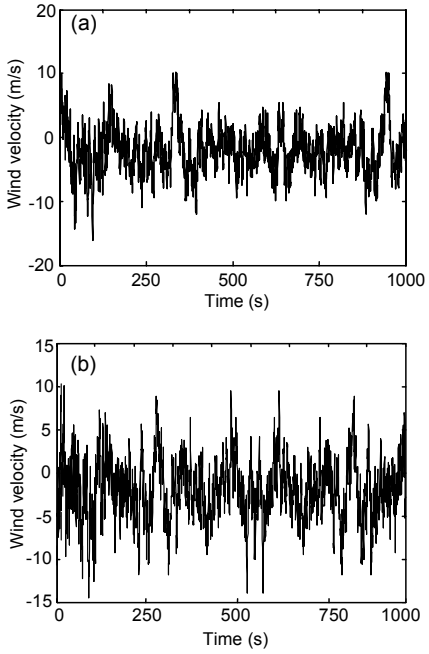

Fig. 2 Wind velocity time series of the 1st (a) and the 10th (b) points by the modified Fourier spectrum method

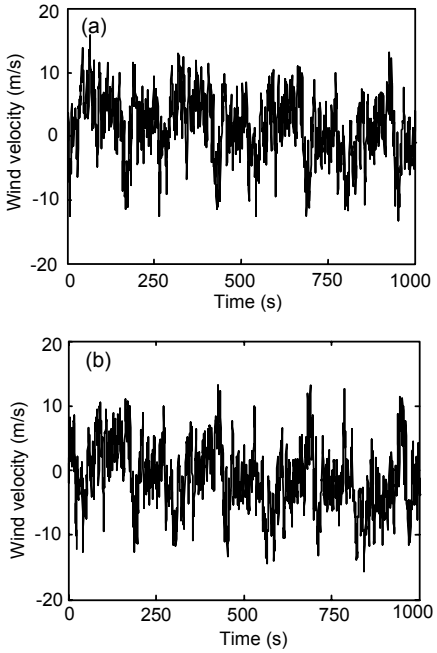

Fig. 3 Wind velocity time series of the 1st (a) and the 10th (b) points by the spectrum representation method (SRM)

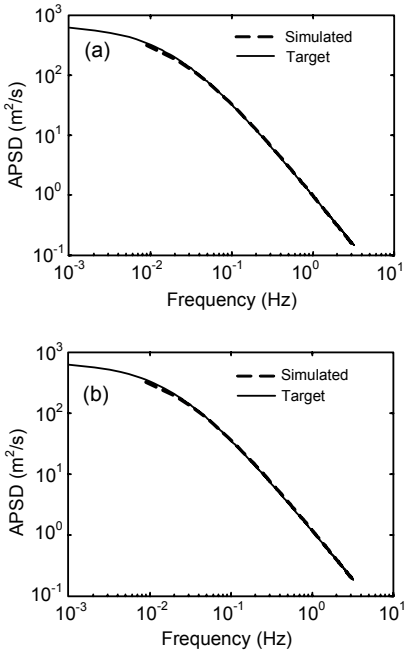

Fig. 4 APSD of the wind velocity time series for the 1st (a) and the 10th (b) points by the modified Fourier spectrum method

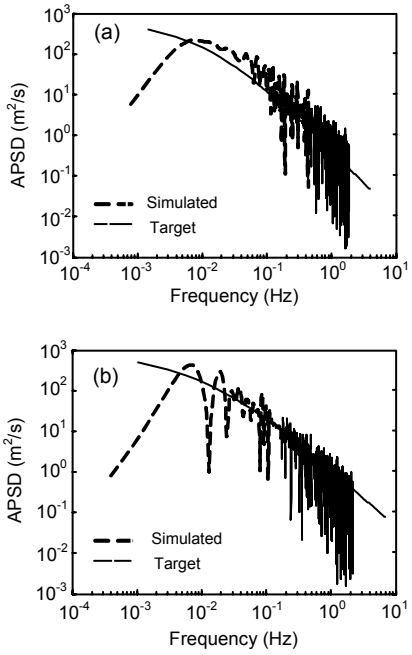

Fig. 5 APSD of the wind velocity time series for the 1st (a) and the 10th (b) points by the spectrum representation method (SRM)

As shown in Figs. 6a and 7a, the CPSD of the wind velocity time history between the 1st and the 2nd points is identically accurate for the MFSM and the SRM, while the MFSM is slightly inferior to SRM in the CPSD of the wind velocity time history between the 9th and the 10th points (Figs. 6b and 7b). The potential reasons may be due to the accumulative error. For example, the phase information of the 2nd point $\phi_2(\omega)$ is determined by $S_{21}^0(\omega)$ and $S_{22}^0(\omega)$ through Eqs. (14) and (15), and phase information of the 3rd point $\phi_3(\omega)$ is determined by $S_{32}^0(\omega)$ and $S_{33}^0(\omega)$, but the contribution of $S_{31}^0(\omega)$ to $\phi_3(\omega)$ is not taken into consideration in order to simplify the calculation process and to avoid the Cholesky decomposition. Consequently, $\phi_3(\omega)$ will have a systematic error. Similarly, the phase information of the 10th point $\phi_{10}(\omega)$ is determined by $S_{10,9}^0(\omega)$ and $S_{10,10}^0(\omega)$, while the contributions of $S_{10,1}^0(\omega)$, $S_{10,2}^0(\omega)$, …, and $S_{10,8}^0(\omega)$ are not taken into consideration. Therefore, $\phi_{10}(\omega)$ will have a larger systematic error. This explains why there is a larger error in the CPSD of the wind velocity time history between the 9th and the 10th points (Fig. 6b) than that between the 1st and the 2nd points (Fig. 6a).

The APSD of the wind velocity time history simulated by the MFSM is clearly an improvement. The accuracy of the auto power spectrum simulated by the MFSM is far better than that simulated by the SRM, and the comparison results are shown in Figs. 4 and 5. The accuracy of the cross power spectrum simulated by modified Fourier spectrum is almost the same as that simulated by the SRM (Figs. 6 and 7). In addition, the other merit of the MFSM is found in the numerical simulation; i.e., the MFSM has a faster calculation speed than the SRM. In this numerical example, the time taken by the SRM is 180 s, whilst that of the MFSM is 30 s. This means that the MFSM is 5 times faster than the SRM in the calculation speed. Therefore, when there are more simulating points, the MFSM will show greater superiority in the calculation speed. This improvement of the calculation speed can be contributed by the avoidance of the Cholesky decomposition in the MFSM. It can be concluded that the MFSM is better than the SRM.

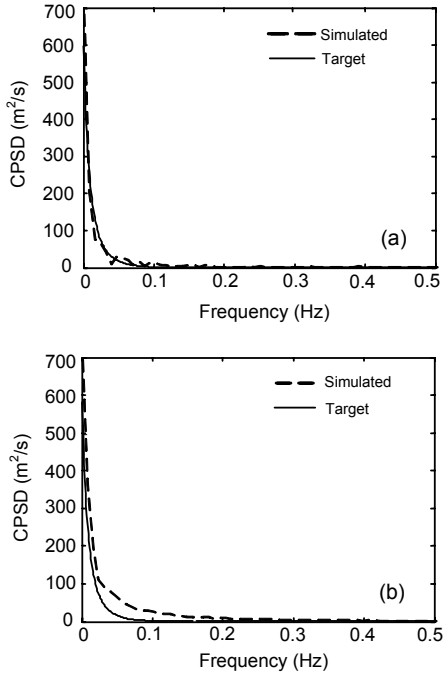

Fig. 6 CPSD of the wind velocity time series for the 1st and 2nd points (a) and the 9th and the 10th points (b) by the modified Fourier spectrum method

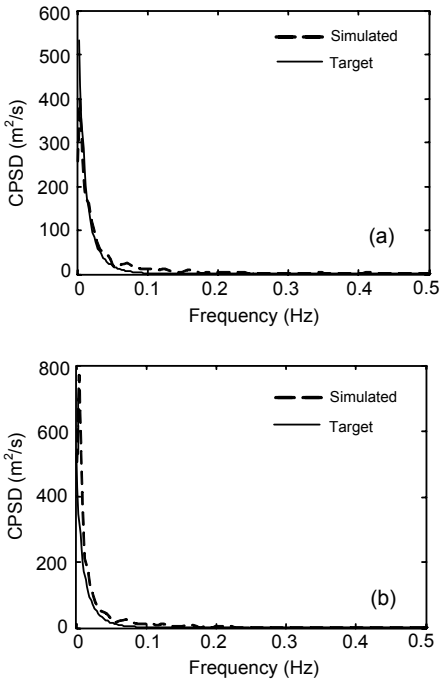

Fig. 7 CPSD of wind velocity time series for the 1st and 2nd points (a) and the 9th and the 10th points (b) by the spectrum representation method (SRM)

5 Conclusions

In this paper, the MFSM is introduced to simulate the stochastic wind field. Numerical example analysis for the modified Fourier spectrum method and the SRM is undertaken. The following conclusions can be obtained.

1. The MFSM has excellent coincidence between the APSD of simulated wind velocity time history and the target power spectral density, and the simulation accuracy is greatly improved compared to SRM.

2. The CPSD of the wind velocity time history simulated by the MFSM is a little higher than the target values. The main cause for this is the accumulative error when determining the phase information.

3. The MFSM shows a great improvement in the calculation efficiency due to the avoidance of the Cholesky decomposition. For large complex structures of many simulating points, the MFSM will show greater superiority.

References

Backström, D., Nilsson, A.C., 2007. Modeling the vibration of sandwich beams using frequency-dependent parameters. *Journal of Vibration and Control*, **300**(3):589-611.

Chondros, T.G., Dimarogonas, A.D., 1989. Dynamic sensitivity of structures to cracks. *Journal of Vibration, Acoustics*, *Stress and Reliability in Design*, **111**:251-256.

Davenport, A.G., 1961. The spectrum of horizontal gustiness near the ground in high winds. *Quarterly Journal of the Royal Meteorological Society*, **87**(372):194-211. [doi:10.1002/qj.49708737208]

Deodatis, G., 1996. Simulation of ergodic multivariate stochastic processes. *Journal of Engineering Mechanics*, **122**(8):778-787. [doi:10.1061/(ASCE)0733-9399(1996)122:8(778)]

Islam, N., Zaheer, M.M., Ahmed, S., 2009. Double hinged articulated tower interaction with wind and waves. *Journal of Wind Engineering and Industrial Aerodynamics*, **97**(5-6):287-297. [doi:10.1016/j.jweia.2009.07.002]

Kaimal, J.C., Wyngaad, J.C., Izumi, Y., Cote, O.R., 1972. Spectral characteristics of surface layer turbulence. *Quarterly Journal of the Royal Meteorological Society*, **98**(417):563-589. [doi:10.1002/qj.49709841707]

Lazzari, M., Vitaliani, R., Majowiecki, M., Saetta, A., 2003. Dynamic behavior of a tensegrity system subjected to

follower wind loading. *Computers and Structures*, **81**(22-23):2199-2217. [doi:10.1016/S0045-7949(03)00291-8]

Li, H.N, Bai, F.L., Li, T., Hao, H., 2011. Response of a transmission tower-line system at a canyon site to spatially varying ground motions. *Journal of Zhejiang University-SCIENCE A (Applied Physics & Engineering)*, **12**(2):103-120. [doi:10.1631/jzus.A1000067]

Mason, M.S., Wood, G.S., Fletcher, D.F., 2009. Numerical simulation of downburst winds. *Journal of Wind Engineering and Industrial Aerodynamics*, 97(11-12):523-539. [doi:10.1016/j.jweia.2009.07.010]

Mazanoglu, K., Yesilyurt, I., Sabuncu, M., 2009. Vibration analysis of multiple-cracked non-uniform beams. *Journal of Vibration and Control*, **320**(4):977-989.

GB 50009-2001. Load Code for the Design of Building Structures. Ministry of Construction of People's Republic of China. China Architecture and Building Press, Beijing (in Chinese).

Miyata, T., Yamada, H., Katsuchi, H., Kitagawa, M., 2001. Full scale measurement of Akashi-Kaikyo Bridge during typhoon. *Wind Engineering*, **89**(9):341-344.

Moustafa, A., Takewak, I., 2009. Use of probabilistic and deterministic measures to identify unfavorable earthquake records. *Journal of Zhejiang University-SCIENCE A (Applied Physics & Engineering)*, **10**(5):619-634. [doi:10.1631/jzus.A0930001]

Samaras, E., Shinozuka, M., Tsurui, A., 1985. ARMA representation of random processes. *Journal of Engineering Mechanics*, **111**(3):449-461. [doi:10.1061/(ASCE)0733-9399(1985)111:3(449)]

Shinozuka, M., Jan, C.M., 1972. Digital simulation of random processes and its applications. *Journal of Sound and Vibration*, **25**(1):111-128. [doi:10.1016/0022-460X(72)90600-1]

Wang, J., Hu, X., 2006. Application of Matlab in Treatment of Vibration Signal. China Water Power Press, Beijing (in Chinese).

Xu, Y.L., Zhu, L.D., Wong, K.Y., Chan, K.W.Y., 2001. Field measurement results of Tsing Ma Suspension Bridge during Typhoon Victor. *Structural Engineering and Mechanics*, **10**(6):545-559.